Applied Geography 136 (2021) 102587

Contents lists available at ScienceDirect

Applied Geography

journal homepage: www.elsevier.com/locate/apgeog

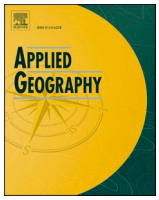

Atmospheric circulation regimes for prescribed burns along the U.S. Gulf of Mexico coast

Wenjia Cao [a,*], Robert V. Rohli [a], Fenglin Han [a], Anthony J. Vega [b], Nazla Bushra [a], John A. Nyman [c]

[a] Department of Oceanography & Coastal Sciences, Louisiana State University, Baton Rouge, LA, 70803, USA
[b] Department of Biology and Geosciences, Clarion University of Pennsylvania, Clarion, PA, 16214, USA
[c] Louisiana State University Agricultural Center, Louisiana State University, Baton Rouge, LA. 70803, USA

ARTICLE INFO

Keywords:
Automated synoptic classification
Atmospheric circulation variability
Bird migration
Prescribed marsh burns
United States Gulf of Mexico coast
Principal components analysis

ABSTRACT

The regional-to-synoptic-scale steering atmospheric circulation is important for advecting energy, mass, and momentum across space, with the near-surface wind being the local manifestation of this circulation. The local winds can affect phenomena of economic, ecological, and/or aesthetic values, such as bird migrations and prescribed burns to restore bird habitats. The purpose of this research is to classify the days from 1979 to 2018 based on circulation patterns near the surface (i.e., 1000-hPa) and at the highest level of airflow affecting bird migration (i.e., 700-hPa), across the Gulf Coast region of the United States. The resulting patterns, derived from Ward's clustering method on rotated principal component scores, are used as input in a fire management plan to restore niches for bird species such as black and yellow rails and mottled ducks. Results suggest that for the (near-surface) 1000-hPa level, a classification system consisting of eight circulation types maximizes the between-group variability while minimizing the within-group variability, with a total of 95.8 percent of the dataset variance explained, and reasonable correspondence with existing manual, subjective and semi-automated techniques. At the 700-hPa level, a system of eight circulation types was derived, explaining 95.05 percent of the dataset variance. In general, the western U.S. Gulf of Mexico arc is more likely than the eastern to respond to synoptic control in the form of weather types, while the eastern region may have more influence from local-to-*meso*-scale land and sea breezes. These results will assist in optimizing the success of controlled burn conditions while enhancing efforts to minimize advection to populated areas.

1. Introduction and background

Fire influences natural vegetation worldwide except Antarctica. Wildfire attracts more public attention but agricultural burning and prescribed fires in natural plant communities probably are more common. Fire is prescribed in natural plant communities to favor some plants and animals over others. Examples include British peatlands (Whitehead, Weald, & Baines, 2021), North American and Australian forests (Black, Hayes, & Strickland, 2020) and Chinese wetlands (Wang, Xu, Wu, Shen, & Cai, 2019).

In the southeastern United States, prescribed fire is used by farmers, foresters and wildlife managers. Of the 40,480 km^2 of rangelands and forests annually burned in the U.S., 61% are in the Southeast (Melvin, 2020). Some forest lands are burned to sustain longleaf pine savanna ecosystems, which occupied over 300,000 km^2 prior to European colonization but now occupies about 12,000 km^2 with all sustained by fire (Van Lear, Carroll, Kapeluck, & Johnson, 2005). In addition, at least 12,390 km^2 of croplands are burned annually in the U.S. with 45% of that occurring in the Southeast (McCarty, Korontzi, Justice, & Laboda, 2009). Much of that burning is for rice and sugar cane in Florida and along coastal Texas and Louisiana, and for cotton throughout the Mississippi River Alluvial Valley from Tennessee to Louisiana (McCarty et al., 2009). Coastal prairie in Texas and Louisiana is also managed with fire to improve wildlife habitat (Feher et al., 2021). Prescribed fires are also commonly used to improve habitat for wildlife in coastal wetlands especially in the Southeast (Nyman & Chabreck, 1995), where the Gulf Coast contains 46% of the 458,000 km^2 of coastal wetlands in the conterminous U.S. and the southeast Atlantic coast contains 37% (Field, Alexander, & Broutman, 1988).

Black et al. (2020) reported that prescribed forest burners in

* Corresponding author.
E-mail address: wcao4@lsu.edu (W. Cao).

https://doi.org/10.1016/j.apgeog.2021.102587
Received 28 June 2021; Accepted 10 October 2021
Available online 14 October 2021

Australia and the U.S. were being asked to burn more area with fewer resources while being challenged by changing climate, shifting demographics, and changing land use patterns. On the U.S. Gulf Coast, anecdotal reports suggest that coastal marsh managers are experiencing increased difficulty meeting agency targets. Such burns generally occur during winter, but during the 1980s, managers preferred to burn prior to cold front passage when southerly winds prevailed so that the marsh surface was flooded by several inches of water. Today, managers generally prefer to wait until after frontal passage because of increased sensitivity to smoke moving northward/inland even though the marsh surface is usually drained by that time (J.A.N. personal observation).

Minimizing fire escape and smoke dispersion into developed areas during prescribed fires depends on the predictability of atmospheric conditions. Reducing smoke impact requires predicting smoke production and dispersion accurately over the range of atmospheric conditions and burn scenarios (Hiscox & Flecher, 2016). Recent work has identified linkages between prescribed burns in the southeastern U.S. and El Niño (e.g., Chiodi, Larkin, & Varner, 2018; Goodrick & Hanley, 2009) and other atmospheric teleconnections (Dixon, Goodrich, & Cooke, 2008). Characteristics of suitable mixing heights and ventilation indices are described in Chiodi, Larkin, Varner, and Hiers (2019).

While such research is welcome and helpful, more research is needed that considers holistic, synoptic circulation patterns as related to prescribed burns. The work by Labosier, Frauenfeld, Quiring, and Lafon (2015) is particularly beneficial in this regard, as it used the pre-existing Spatial Synoptic Classification scheme (Davis & Kalkstein, 1990; Kalkstein, Nichols, Barthel, & Greene, 1996; Sheridan, 2002) to identify preferences for wildfires to occur in the south-central U.S. under varying synoptic air-mass types.

Understanding the major seasonality and variability patterns of near-surface and steering atmospheric circulation is also an important component of atmospheric environmental planning for such burns. Labosier et al. (2015) provided an excellent use of a circulation-based system that might produce patterns resembling what a fire manager would see on a weather map. Such a system is preferable over air-mass based classifications for some applications. Characterizing and classifying atmospheric circulation into a discrete number of patterns provides another fundamental basis for understanding the synoptic climatology, which then facilitates the exploration of relationships between atmospheric circulation and regional environments that exist within those discrete types (Beck, 2015). Eigenvector analysis is the most commonly accepted approach for identifying the major modes of variability in circulation. When the eigenvector analysis is paired with classification techniques that simultaneously maximize between-group variability and minimize the within-group variability, a robust atmospheric circulation classification will be generated (Yarnal, 1993).

In climatology, principal components analysis (PCA) is the most common eigenvector analysis method. The technique allows an observed set of features to be transformed into a smaller set of linear combinations that can explain most of the original dataset's variance (Jolliffe & Cadima, 2003). Moreover, the orthogonal modes of variability ensure that components are uncorrelated, thereby enabling its application to maximize the information of interest contained in the extracted features (i.e., eigenvector-based feature extraction for classification). PCA is also frequently used as a method of reduction of dimensionality, which also measures the nonlinearity of various data sets (e.g., Zscheischler, Mahecha, & Harmeling, 2012).

Rotation of PCA results involves a linear transformation of conventional PCA output to improve the representation and accuracy for certain types of applications, including eigenvector-based map-pattern classification (Yarnal, 1993). In the commonly used rotated PCA (RPCA) technique known as varimax (Richman, 1986), the eigenvectors are weighted by the square root of the eigenvalues and the rotation ensures that the resulting patterns are orthogonal, thereby explaining unique components of variability (Jolliffe, 1995). Orthogonal rotation ensures accuracy and robustness in identifying the modes of variability by circumventing spurious "Buell sequences" (Buell, 1979), which occur when maximum loadings of the first principal component (PC) are near the center of a spatial distribution (i.e., where a dataset's points are most likely to be related most directly to variability elsewhere in the dataset), and loadings of the next four PCs peak in each corner of the distribution. Barnston and Livezey (1987) compared monthly PCA and varimax-RPCA patterns in the lower-to-middle troposphere with their corresponding known patterns of atmospheric pressure (and therefore flow) variability, such as El Niño/Southern Oscillation, with sensitivity tests used to illustrate the significant reductions in sampling error. RPCA showed great success over the conventional method, perhaps due to the relaxation of the geometrical and mathematical constraints in the process of extracting features. The varimax technique is frequently used in the atmospheric science literature for similar studies of atmospheric circulation variability (e.g., Raziei, Bordi, Santos, & Mofidi, 2013).

The mathematical algorithm of PCA is derived using a series of complicated matrix transformations in a high-dimension coordinate, geometrically projecting them onto lower dimensions. Because it is explained in detail in many other sources, the method will only be introduced briefly here. In the case of a data matrix X with a dimension of m rows of samples and n columns of features, a projection matrix W is composed of m rows and m columns containing the eigenvectors of XX^T. Thus, X can be written as Eqn 1:

$$X = W\Omega V^T \tag{1}$$

where the rectangular diagonal matrix Ω has a dimension of $n \times n$ and the rectangular orthogonal matrix V also has a dimension of $n \times n$. The PCs are calculated by Eqn 2

$$Y = W^T X = W^T W\Omega V^T = \Omega V^T \tag{2}$$

and the variance is maximized (Zscheischler et al., 2012).

PCA is applied in this work to make use of its properties of: 1) identifying the best linear approximation of mean square of the matrix; 2) deriving extracted features that are uncorrelated; 3) maximizing the explained variance of the extracted features; and 4) maximizing the information obtained from the extracted features (eigenvector-based feature extraction for classification). PCA distributes high weights to features with higher variabilities, with the caveat that results can be affected significantly by selections of domain, grid, scaling, and time, in terms of climate analysis. The latter justifies additional circulation-based research at multiple levels in a region.

Applications of PCA in the context of climatology and meteorology have a rich history. For example, Overland and Preisendorfer (1982) used PCA to optimize the signal-to-noise ratio in identifying common low-pressure storm (i.e., cyclone) tracks. Richman and Lamb (1985) examined the climate pattern on 3-day and 7-day summer rain periods and explained the entire domain variance by both unrotated PCA and varimax-rotated PCA. The rotated results showed more domain-correlated characteristics than the unrotated and presented considerable potential utility for study of climate variation and change. Pandžić (1988) regionalized precipitation zones using PC loadings and compared the results with those calculated based on Köppen's (1884) nearly universally-used thermal and water-balance-based climatic classification system. Daigle, St-Hilaire, Beveridge, Caissie, and Benyahya (2011) applied PCA in describing regional characteristics and deviations from low-flow hydrological regimes.

Many examples of eigenvector- and particularly PCA-based analysis for analyzing atmospheric circulations exist (e.g., Kostopoulou & Jones, 2007; Trenberth, Stepaniak, & Caron, 2000; Yarnal, Comrie, Frakes, & Brown, 2001). Atmospheric circulation variability has also been the focus of several PCA-based studies along the Gulf of Mexico (GoM) coast in recent years. Rohli and Rogers (1993) identified the major modes of 700-hPa-level atmospheric flow that contribute to citrus freezes along the U.S. GoM coast. Vega, Rohli, and Henderson (1998) examined mid-tropospheric flow variability over the GoM during El Niño and La

Niña. Rohli and Henderson (1998; 2002) contrasted 500-hPa flow patterns that directed high-pressure systems (i.e., anticyclones) of continental vs. Pacific origin to the GoM coast. Rohli, Russo, Vega, and Cole (2004) derived circulation regimes that affect tropospheric ozone mixing ratios over Louisiana.

One study is of particular interest here, because of their explicit goals of classifying surface weather circulation regimes focused on New Orleans, Louisiana. Muller (1977) developed a subjective, manual classification system (i.e., without using PCA or related eigenvector techniques) by examining daily weather maps and grouping them according to pre-conceived circulation types. That approach has been applied extensively in the study region over the years (e.g., Dagg, 1988; Engle et al., 2008; Keim & Muller, 1992; Muller & Jackson, 1985; Wang, Ransibrahmanakul, Tuen, Wang, & Zhang, 1995). Lewis and Keim (2015) developed a "hybrid" (i.e., part-subjective and part-objective; Frakes & Yarnal, 1997) approach by conducting correlation-based automated classification of daily weather types based on "key days" that represent prototypes of each of Muller's (1977) eight categories. Lewis and Keim (2015) were able to replicate Muller, (1977) daily calendar of patterns reasonably well, over the 1981 to 2001 period – the period from which the Muller (1977) system had been updated. One important difference between the current work and that of Lewis and Keim (2015) is that the latter study's reliance on correlation-based classification does not take into account the holistic dataset variability. Eigenvector-based techniques alleviate this shortcoming.

The goal of this research is to develop a synoptic climatology of surface and steering atmospheric circulation on the U.S. GoM Coast, an area where prescribed marsh burns are frequently used as part of an avian wildlife management plans, in one of the world's most diverse, productive avian environments. The surface results are validated by comparison with the subjective method of Muller (1977) and the hybrid method of Lewis and Keim (2015).

2. Data and methods

Geopotential height fields (which correspond to pressure patterns) at the 1000-hPa and 700-hPa levels were acquired from the fifth-generation European Center for Medium-Range Weather Forecasts (ECMWF) Reanalysis version 5 (ERA5; Copernicus Climate Change Service (C3S), 2017) at 0.25° × 0.25° resolution. The study area includes the U.S. Southeast and adjacent GoM, bounded by 100°W, 40°N, 75°W, and 20°N, for 1200 UTC and 1800 UTC from January 1, 1979 to December 31, 2018. For each level of analysis, the original data were standardized into z-scores by grid point, by time of day and Julian day of the year, for the 40 observations (i.e., one per year) at each grid point (excepting 29 February, which had only ten observations). This approach facilitates comparison across space and time by identifying departures from mean conditions at that point and a given time of day and year.

The 1000-hPa pattern is indicative of surface atmospheric circulation which determines local wind speeds and direction, thereby influencing potential fires. The 700-hPa level (which corresponds to 2.9 to about 3.3 km in altitude) is important as it represents the highest atmospheric level affecting bird migrations (Duerr et al., 2015). Also, it is usually near the zone of maximum thermal and moisture advection, both of which could affect the fire features and spread. In addition, the 700-hPa level is sufficiently high to characterize the broad-scale steering circulation (usually peaking near 5.2 km in elevation) yet also sufficiently low to identify variability associated with the regional-scale low-level jet streams that frequently occur in the GoM and Caribbean areas near 1–2 km in altitude (Mo & Berbery, 2004).

S-mode PCA (Richman, 1986; Jolliffe, 2002), meaning that the input data matrix consists of gridded data along the columns and observation times (twice-daily, at 1200 and 1800 UTC) along the rows, was implemented on the correlation-based data matrix (Jackson, 2005) to generate an eigenvector-based map-pattern classification (Yarnal, 1993)

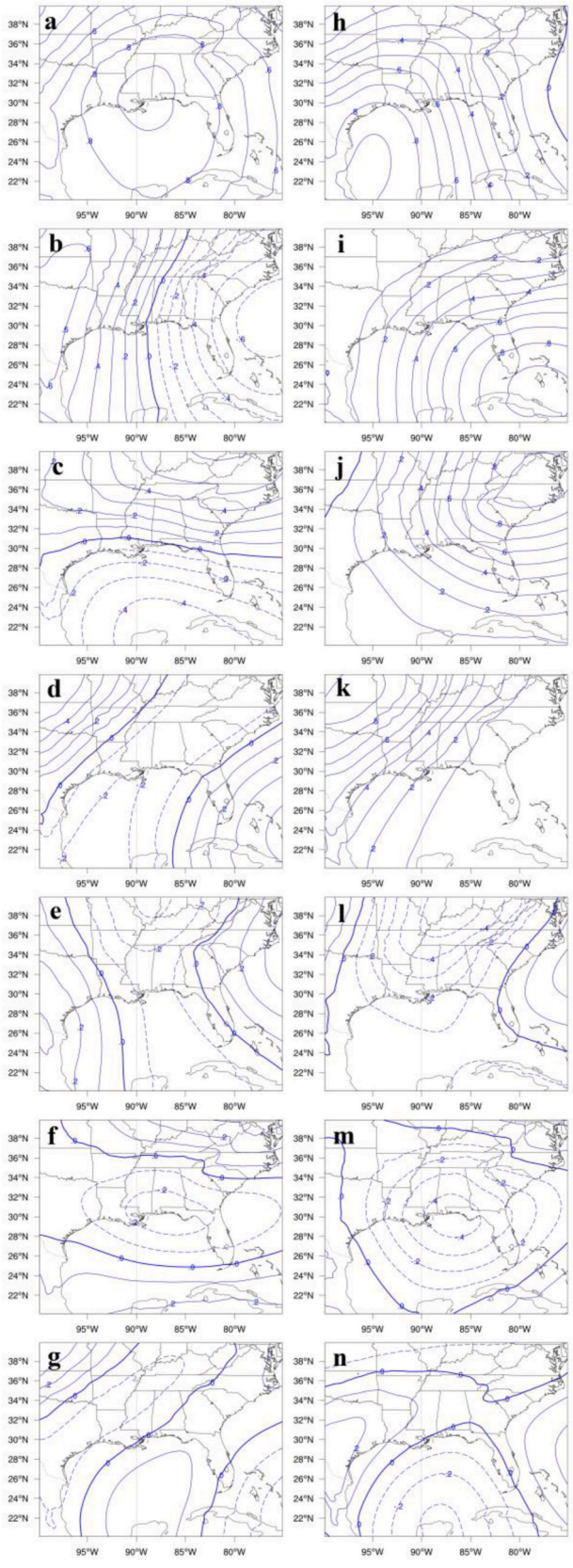

Fig. 1. Loadings maps for the seven retained unrotated (a–g) and rotated (h–n) components in the S-mode PCA for 1000-hPa-level geopotential height data.

at each geopotential height level. The S-mode format allows for the PCA-output eigenvector loadings matrix to have a format of stations along the rows by PC along the columns, meaning that the loadings represent spatial variability, and can therefore be mapped by PC. Furthermore, the format also allows for the PCA-output eigenvector scores matrix to have the format of time along the rows and PC along the columns, which allows for the scores to be analyzed as a time series by PC. Thus, S-mode PCA allows for the simultaneous analysis of spatio-temporal variability in the data set, for the 1000-hPa and (in a separate analysis), 700-hPa levels. For the 1000-hPa analysis, a scree plot (Cattell, 1966) of eigenvalues by component revealed a slope "break" after the seventh component, suggesting that seven components (representing 53.8, 18.6, 10.6, 4.8, 2.6, 1.8, and 1.3 percent, respectively, for a total of 93.4 percent of the dataset variance) should be retained for further analysis in a varimax-RPCA. Similarly, the 700-hPa analysis also revealed that seven components, explaining 54.4, 17.5, 14.3, 3.6, 2.9, 2.4, and 1.1 percent, respectively, for a total of 96.1 percent of the dataset variance, should be retained.

For each level, the rotated component loadings were mapped to identify the main regions of geopotential height (and therefore corresponding flow) variability. Moreover, each temporal observation (i.e., 1200 UTC or 1800 UTC for each day) in the RPCA scores matrix is represented in seven-dimensional space (one dimension per PC) and input into a cluster analysis (Gore, 2000) to identify the main circulation types, for each level of analysis, separately. The clusters of temporal observations are formed by minimizing the within-group variance while maximizing the between-group variance, with each cluster of days representing a circulation type. Ward's (Ward, 1963) algorithm was selected because previous research for year-round synoptic typing (Yarnal, 1993, p. 80) suggests that it may be optimal, perhaps because it provides a compromise between techniques that agglomerate clusters of vastly different numbers of observations and those that are biased toward generating clusters with similar numbers of observations. The number of circulation types derived from the clusters is based on subjective analysis of the dendrogram. For both the 1000-hPa and 700-hPa levels, composite (i.e., mean) geopotential height maps of each 1200 UTC or 1800 UTC observation having a given circulation type are generated. Additionally, interannual variation and monthly average variation are also analyzed. Version r2019a of MATLAB and R are used in these methods. Our approach of PCA in combination with cluster analysis is well-supported in the literature, and has been found to outperform self-organizing map (Liu and Weisberg, 2005, 2011) approaches for identifying variations in the spectral content of seismicity as related to changes in volcanic activity (Unglert, Radić, & Jellinek, 2016).

3. Results

a. Principal Component Loadings and Centers of Height (Pressure) Variability

Maps of the unrotated PCA loadings on the 1000-hPa analysis (Fig. 1a–g) show a "Buell sequence" bullseye in the middle in the first PC and on the edges of the next several PCs, suggesting a need for rotation to reveal the "real" spatial pattern of variability in the 1000-hPa geopotential height (and therefore flow) instead of an artifact of domain shape. The bullseye in the middle of the domain in the first component is symptomatic of a need to rotate because the highest explained variance in most spatial datasets will be in the middle. This is because the points in the center of the study area are most likely to be influenced by variability in the other data points. By contrast, the bullseyes shown by the mapped pattern of loadings for the seven varimax-rotated components represent the "real" spatial variability explained by the PCs, as they yield a spatial pattern that appears typical of regional-scale pressure variability (Fig. 1h-n).

After rotation, the seven retained components account for 23.5, 16.8,

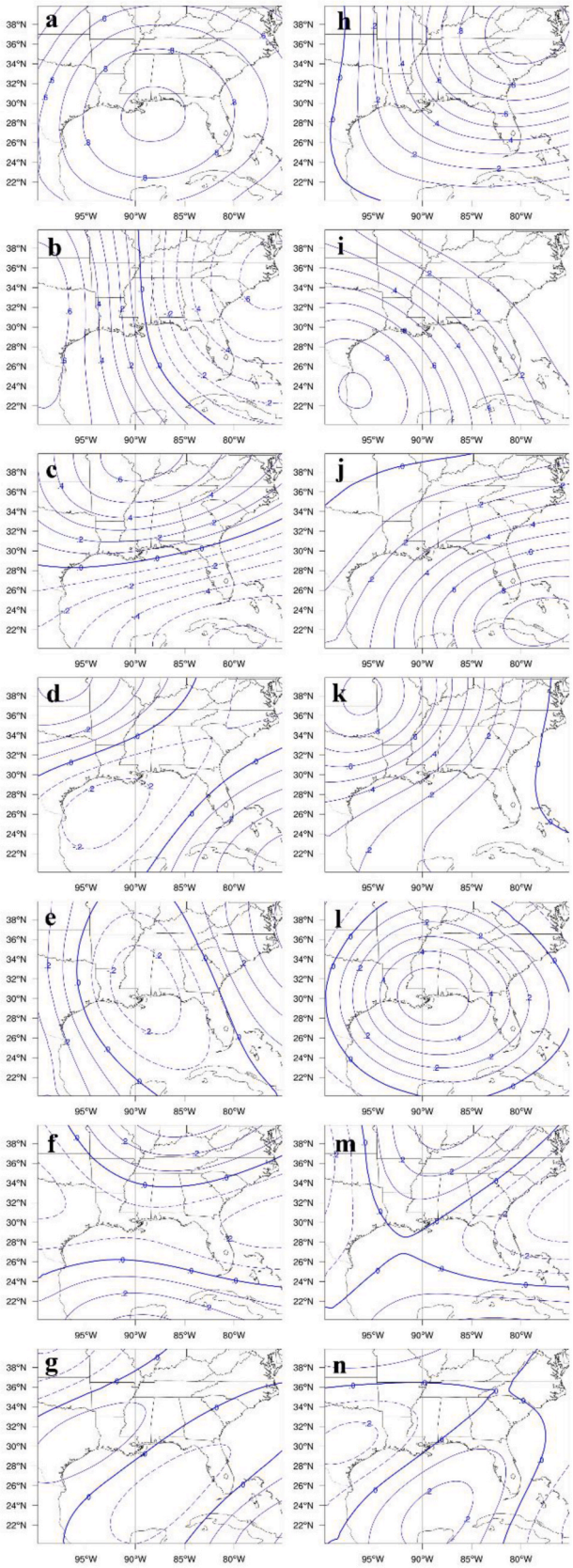

Fig. 2. As in Fig. 1, but for the 700-hPa level.

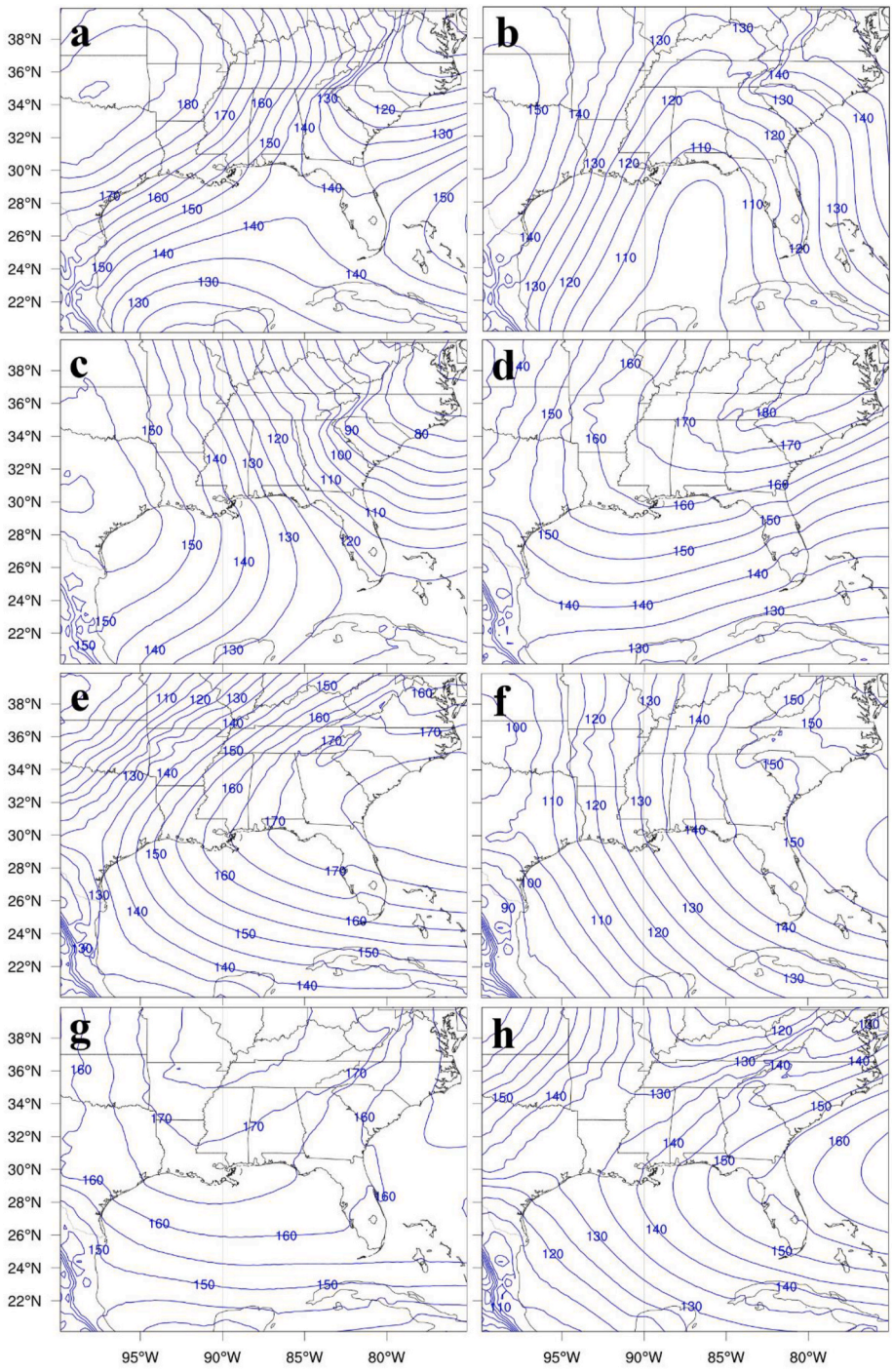

Fig. 3. Composite 1000-hPa geopotential height maps, by circulation type.

13.0, 12.0, 11.2, 9.9, and 7.0 percent of the data set variance, respectively.

In the positive (i.e., depicted) component phase, rotated PC1 (RPC1; Fig. 1h) represents height variations consistent with a surface anticyclone in the western GoM. The inverse phase (flipping the loadings to negative as the PCA-generated signs are arbitrary) of the pattern is associated with a tropical or mid-latitude cyclone in the western Gulf. RPC2 (Fig. 1i) suggests an extension of the Bermuda-Azores subtropical anticyclone (BASA) or a departing migratory mid-latitude anticyclone centered over the southwestern North Atlantic and Caribbean. The opposite pattern suggests a departing mid-latitude (frontal) cyclone or a tropical cyclone centered over the action center. RPC3 (Fig. 1j) depicts an action center over the Mid-Atlantic U.S. that aligns with a migratory anticyclone (mid-latitude cyclone) in the positive (negative) component phase. RPC4 (Fig. 1k) is reminiscent of a strong continental anticyclone (positive phase) or mid-latitude cyclonic center (negative phase) moving eastward through the Great Plains. The loadings pattern for RPC5 (Figure 1l) suggests an approaching anticyclone in the positive phase, with the negative phase supporting a large approaching cyclone. RPC6 (Figure 1m) shows an action center of negative values, thereby depicting lowered pressures in the region. Such a situation aligns with a tropical or mid-latitude cyclone in the positive phase of the loadings pattern, or an anticyclone centered over southern Mississippi, Alabama, and western Florida in the inverse loadings pattern. Finally, RPC7 (Figure 1n) shows

the study area between low-pressure areas that occur north and south of the region. The opposite loadings pattern places the study region between opposing high-pressure regions.

The spatial pattern of unrotated PCA-generated loadings for the 700-hPa analysis also displays the classic Buell sequence (Fig. 2a–g), and varimax rotation after retaining the first seven components again identifies more realistic expressions of the atmospheric circulation variability. Specifically, in the positive loadings phase RPC1 (Fig. 2h) suggests an anticyclone centered over the Mid-Atlantic states, commensurate with the surface pattern denoted in Fig. 1j. The inverse loadings phase shows a reduced heights action center, thereby indicating a migratory cyclone. RPC2 (Fig. 2i) indicates an action center over the western GoM, corresponding to the surface pattern shown in Fig. 1h). In its positive mode, the pattern indicates an anticyclone, or an extension of the BASA over the western GoM. The inverse phase aligns with cyclones in the western GoM. RPC3 (Fig. 2j) shows an action center over Cuba and the Bahamas. The positive loadings phase indicates an extension of BASA over the study area, or a departing cool-season anticyclone. The inverse loadings mode indicates lowered heights indicative of a cyclone of either mid-latitude or tropical origin. RPC4 (Fig. 2k) is Great Plains continental anticyclone or cyclone moving eastward across the study domain. Such a pattern aligns with the surface pattern depicted in Fig. 1k. RPC5 (Figure 2l) suggests a strong variability response in the center of the study domain. The positive loadings mode indicates raised heights and high-pressure, while the opposite phase aligns with lowered heights that accompany a strong cyclone. The pattern corresponds to the surface pattern shown in Figure 1m. RPC6 (Figure 2m) indicates a meridional pattern through the U.S. Midwest to central Gulf South, perhaps associated with polar front jet stream ridging (troughing) in the positive (negative) component phase. Finally, RPC7 (Figure 2n) depicts height/pressure anomalies of the same sign (i.e., two anticyclones or two cyclones), existing simultaneously over the western and.

Eastern boundary of the study area and separated by a height/pressure feature of opposite sign centered over the GoM.

b. 1000-hPa Circulation Patterns

A dendrogram based on cluster analysis on the seven-dimensional RPCA scores matrix produced eight optimal 1000-hPa circulation types. Fig. 3a–h shows the composite 1000-hPa geopotential height (corresponding to pressure) patterns for all days from 1979 to 2018 in each circulation type. Type a (Fig. 3a) indicates a large strong continental anticyclone covering most of the northwestern part of the domain, with a front from Chesapeake Bay to the GoM just off the U.S. east coast, and a weak BASA. Near the area of potential prescribed burns, Louisiana, Mississippi, and Alabama experiences a generally cool, dry wind from the northeast under such circumstances, while coastal Texas experiences a more humid onshore wind. Type b (Fig. 3b) indicates a strong tropical or sub-tropical elongated low-pressure (likely frontal) zone extending through the GoM with evidence of extending to western Florida. Louisiana and coastal Texas experience a strong pressure gradient behind the frontal area, and perhaps overrunning with northeasterly winds from the counter-clockwise flow wrapped around the low-pressure center, and precipitation. At the same time, Florida experiences warm, humid southerly winds ahead of the front. Type c (Fig. 3c) is similar to Type a but with a stronger high pressure dominating the western part of the study area, with the front generating cool, dry winds from the northwest for most of the U.S. GoM coast. Type d (Fig. 3d) features a large, strong anticyclone over the Appalachians. The clockwise circulation around the high produces a humid east to southeasterly airflow over much of the U.S. GoM coast, providing onshore flow to Texas and offshore flow to peninsular Florida's GoM coast. Type e (Fig. 3e) contains a westward-

Protruding band of the BASA, with the western GoM coast experiencing warm, humid winds from the south and peninsular Florida

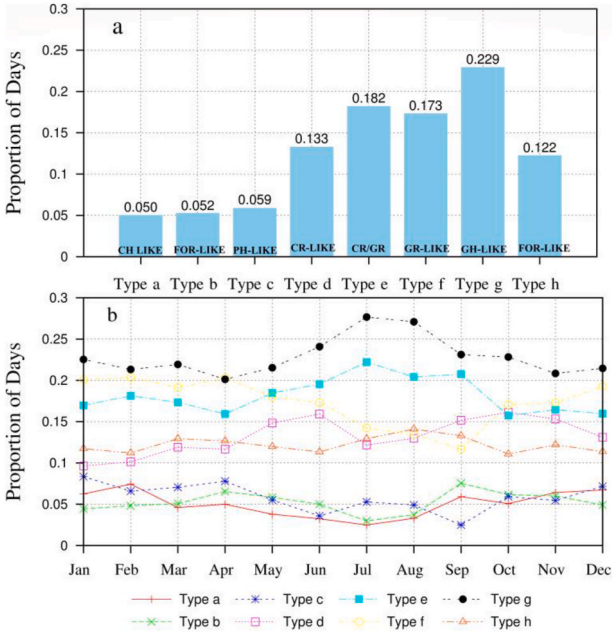

Fig. 4. Total frequency and monthly variation at the 1000-hPa level, by circulation type.

subjected to easterly winds. Type f (Fig. 3f) indicates a strong height (i.e., pressure) gradient, with isohypses oriented from north to south. Such a pattern suggests warm, humid wind being pushed northward across the northern GoM coast, with the higher heights/pressures to the east indicating BASA expansion a strong downstream mid-latitude anticyclone. Either condition produces southeasterly or southerly advection of humid air across the entire U.S. GoM coast in a "return" flow event (Crisp & Lewis, 1992; Lewis & Crisp, 1992). Type g (Fig. 3g) indicates high pressure over eastern Missouri, southern Illinois, and western Kentucky, with a mid-latitude wave cyclone already moved out to the Atlantic, giving most of the U.S. GoM coast weak easterly or southeasterly flow, which would be onshore everywhere except the Florida peninsula. Type h (Fig. 3h) indicates a cold front situated from the central Midwest through eastern Texas, with the U.S. GoM coast situated in the warm sector of the mid-latitude cyclone. Such a synoptic situation produces southerly (i.e, onshore) flow for the Louisiana, Mississippi, Alabama, and Florida panhandle ahead of the approaching front and around the anticyclone to the east.

c. Comparison to Muller, (1977) Surface Circulation Types

The surface patterns of the present study are reminiscent of the circulation types identified for the central GoM coast by Muller (1977), whose classification extended from the 1970s to 2001. Types a, b, and c (Fig. 4a–c) are all "behind the front" patterns, resembling Muller, (1977) "Continental High (CH)," "Frontal Overrunning (FOR)," and "Pacific High (PH)" types, respectively. Type d (Fig. 3d) resembles Muller, (1977) "Coastal Return (CR)" pattern, while Type e (Fig. 3e) represents a transition between Muller, (1977) CR type and Type f (Fig. 3f), the latter of which is reminiscent of Muller, (1977) "Gulf Return (GR)." The weak geopotential height gradient and location of the geopotential height contours (i.e., isohypses) gives Type g (Fig. 3g) several of the distinguishing features of Muller, (1977) "Gulf High (GH)" pattern, though it is displaced northward here, perhaps suggestive of a GH/CH combination. Type h (Fig. 3h) closely resembles Muller, (1977) "Frontal Gulf Return (FGR)" pattern. Muller, (1977) "Gulf Tropical Disturbance (GTD)" is scarcely represented in the present classification, but Type b appears to accommodate cases of low pressure over the Gulf that would include the GTD type. Moreover, our "compromise" selection of Ward's

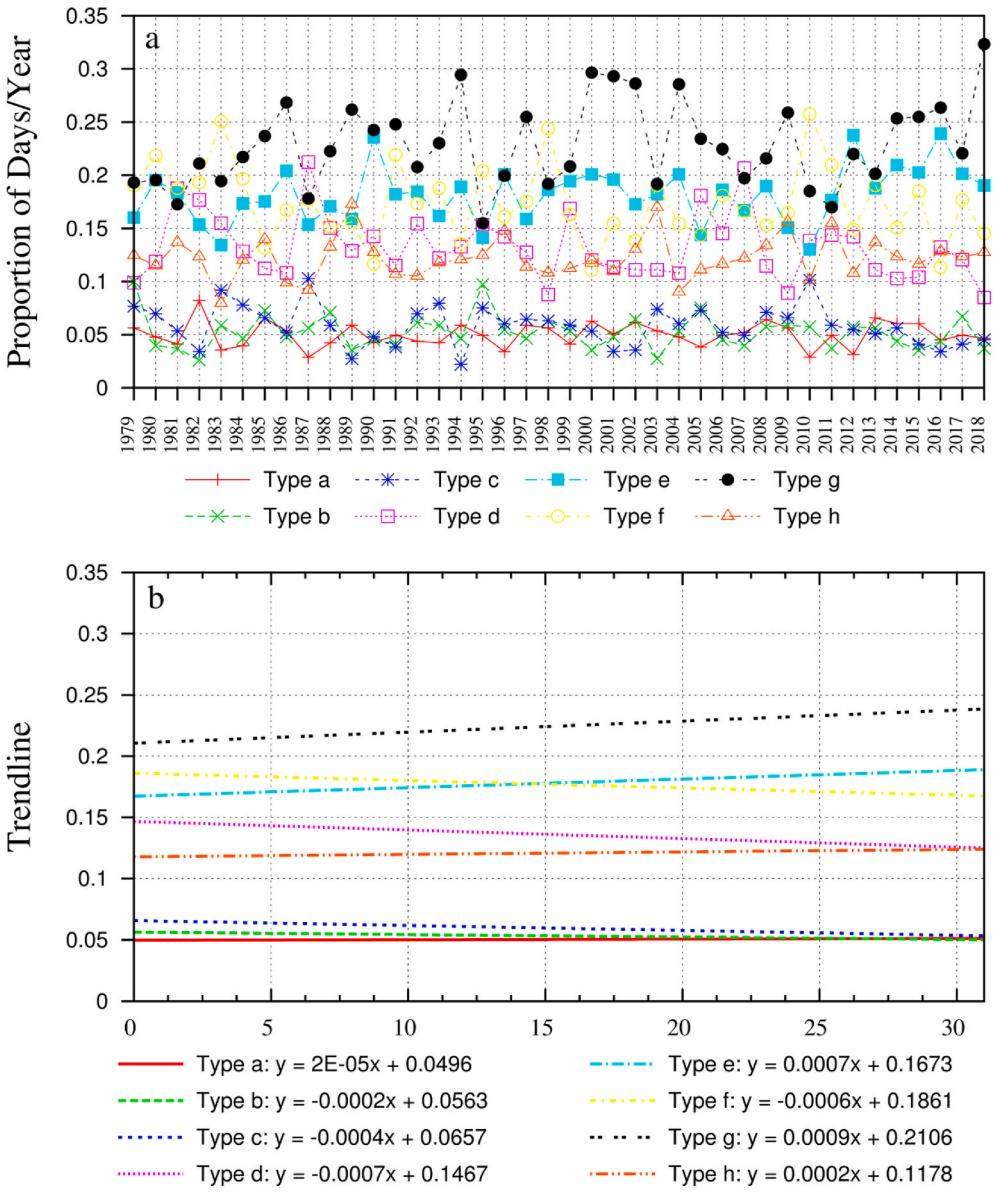

Fig. 5. Interannual frequency variation and linear trends, by 1000-hPa-level circulation type.

(1963) clustering algorithm over others that give outliers more weight in the clustering procedure, such as complete-linkage (Yim & Ramdeen, 2015), may explain this result. The study classification results appear to validate, and be validated, by Muller, (1977) surface-based types, focused on New Orleans. Differences may be attributable to the subjectivity involved in the manual classification, the choice of cluster analysis, spatial differences in the study area, and/or climatic change since the manual classification.

d. Frequencies of 1000-hPa Circulation Patterns

Total and monthly frequencies of all eight 1000-hPa circulation types are shown in Fig. 4a–b. The proportion of total days by cluster ranges from 5.0 (Type a - the CH-like pattern) to 22.9 (Type g – GH-like pattern), respectively (Fig. 4a). These extreme proportions may be partially explained by the fact that Type g also includes many features of Muller's CH type, thereby decreasing frequencies of Type a while increasing those of Type g. The slightly elevated proportions for Types d (CR), e (CR/GR), and g (GH) in summer suggest the influence.

Of BASA at the time of year when it is most intense. The FGR-like pattern (Type h) is more common when fronts trailing from mid-latitude wave cyclones lack the steering mechanisms to penetrate through the region. Types a (CH), b (FOR), c (PH), and f (GR) are more frequent in the cold season. The results support those of Muller (1977), as frequencies of the CH, FOR, and PH types are more abundant in winter, as the study area would be more likely to be positioned "behind the front" in the cold season. The GR type is relatively common year-round, according to both Muller (1977) and this analysis. However, it tends to mirror the FGR in frequency; at times of year when cold fronts cannot penetrate to the Southeast quite so easily (i.e., summer), FGR (i.e., the pre-frontal flow type) is more common. At times of year when cold fronts can pass through the region without stalling before reaching the U.S. Southeast (i.e., winter), FGR frequency decreases and GR frequency increases.

The interannual variation of the percentage of total observations by year represented by each 1000 hPa type is shown in Fig. 5. In general, Types g, e, h, and a (the GH-, CR-/GR-transition, FGR-, and CH-like types, respectively) display increasing temporal frequencies, while Types d (CR), f (GR), c (PH), and b (FOR) have decreasing frequencies. However, the only statistically significant linear temporal trend is for

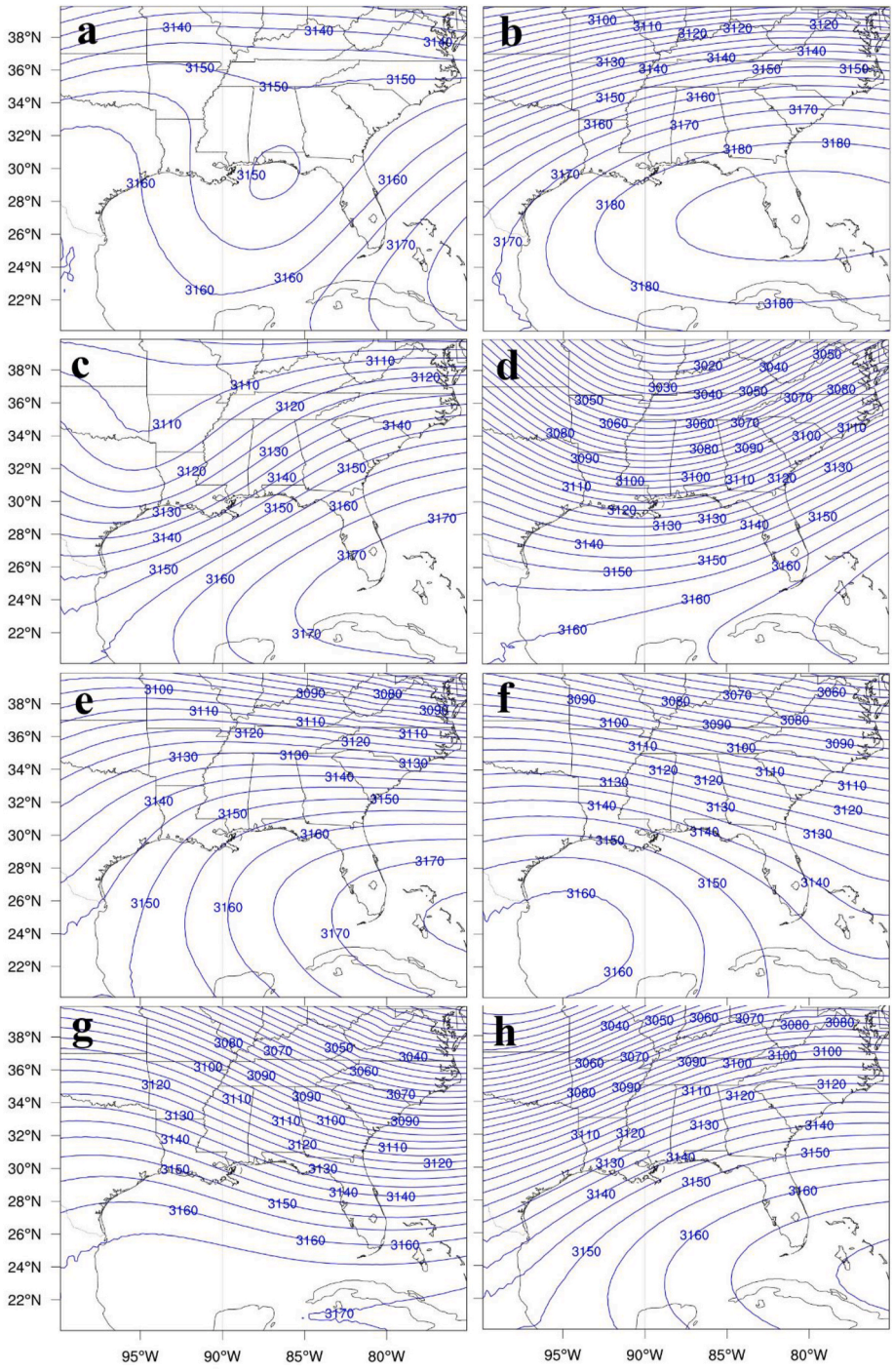

Fig. 6. As in Fig. 3, but for the 700-hPa level.

Type e ($p = 0.0495$, $r = 0.312$), with a suggestion of possible significance for Types d ($p = 0.1019$, $r = 0.262$) and g ($p = 0.1038$, $r = 0.261$). The statistical insignificance of the temporal trends in frequency for FGR (Type h; $p = 0.4098$, $r = 0.134$) and FOR (Type b; $p = 0.4108$, $r = 0.134$) suggests that there is no convincing evidence that fronts are increasingly likely to stall north or northwest of the study area during the study period. Likewise, the absence of significant linear temporal trends in Types b, c, and a ($p = 0.4108$, $r = 0.134$, $p = 0.1732$, $r = 0.212$, and $p = 0.8821$, $r = 0.024$, respectively) corroborates this finding; these three types are associated with a post-cold-frontal passage situation involving either an anticyclone (Types a and c) or overrunning cloud coverage (Type b). It is possible that increased frontal stalling over time could increasingly cause "runs" of consecutive days of a particular weather type, which might offset any decrease in weather type frequencies owing to a decreased rate of frontal passages. However, such a scenario is unlikely because of the simultaneous presence of both positive and negative statistically significant trends among the weather types, all of which are components of the mid-latitude wave cyclone.

e. 700-hPa Circulation Patterns

Rotation of the first seven components yields explained variances of 24.4, 13.0, 12.9, 15.3, 14.3, 9.4, and 6.8, percent, respectively. Composite 700-hPa geopotential height patterns for days in each circulation

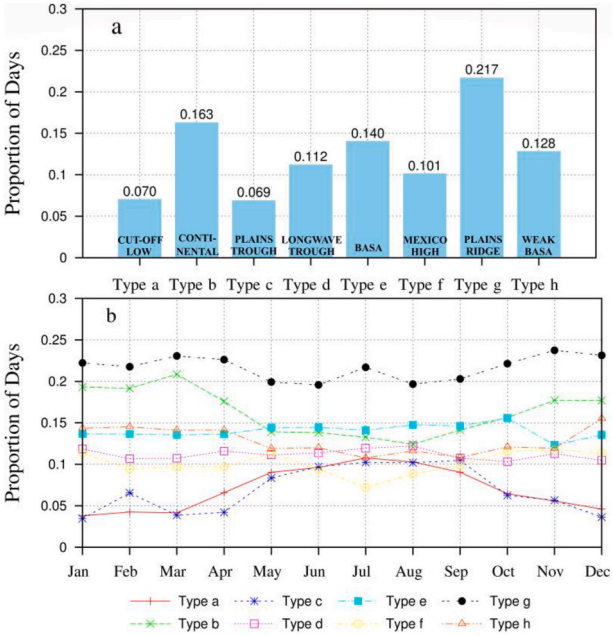

Fig. 7. As in Fig. 4, but for the 700-hPa level.

type are shown in Fig. 6a–h. The types described here were.

Derived independently from those **a**t the 1000-hPa level and therefore the patterns do not correspond directly between the two levels. Type a (Fig. 6a) indicates a trough at the U.S. GoM coast, with a weak pressure gradient and a "cut-off low" (as is evidenced by the enclosed area of low (i.e., 3150 m) geopotential heights over the Alabama/Florida GoM coast) isolated from the west-to-east flow to the north. Type b (Fig. 6b) indicates a strong (as indicated by the high 700-hPa isohypes) continental anticyclone that dominates the GoM and peninsular Florida. It is unlikely to be the 700-hPa representation of the BASA because of its prevalence during the cold season and because of the suggestion of enclosed isohypses rather than an extension from the east. Type c (Fig. 6c) suggests a trough over the Great Plains, accompanied by the BASA extending toward the southeastern section of the domain. Type d (Fig. 6d) features an intense longwave trough that dominates the study area, with a cyclone likely positioned over the western Great Lakes. Type e (Fig. 6e) is similar to Type b (Fig. 6b) but may represent the BASA rather than a continental anticyclone because the isohypes seem to extend to the BASA position. Type f (Fig. 6f) indicates a high–pressure ridge or anticyclone located over Mexico, again with strong height/pressure gradients in the northeastern corner. Type g (Fig. 6g) shows a Great Plains ridge with simultaneous trough over the eastern U.S. and a strong height/pressure gradient north of the GoM. Type h (Fig. 6h) resembles Type e, but with a weaker BASA, with intense height gradients over most of the domain.

f. Frequencies of 700-hPa Circulation Patterns

Total and monthly frequencies of all eight 700-hPa circulation types are shown in Fig. 7a–b. Annual frequencies range from 6.9 (Type c – Plains trough) to 21.7 (Type g – Plains ridge) percent of all days. The dominance of ridging over the Plains suggests the known preference for.

Ridges to be locked in place over the western mountain cordillera of North America, as the conservation of potential vorticity causes air parcels descending the eastern slopes to gain anticyclonic (i.e., clockwise in the Northern Hemisphere) vorticity, as occurs when air flows around a ridge. Type b (CH) was the second-most common among all eight types, with a value exceeding 16 percent of all days.

Seasonal patterns can also be observed based on monthly variation. Types b, f (Mexico high), g, and h (weak BASA) displayed relatively higher frequencies in cold months than warm months. Thus, the 700-hPa equivalents of the CH, and perhaps, the PH types (i.e., Types b and f) indeed also show more influence in the cold season. On the other hand, Types a (GoM cut-off low) and c (Plains trough) favor the warm months. The former suggests the inclusion of the 700-hPa signature of Gulf tropical cyclones in Type a, as Hurricanes Katrina, Gustav, and others fell into this category of 700-hPa flow. Type b was characterized by the most distinct seasonality, while Types d (Longwave trough) and e (BASA) showed relatively small fluctuations through the year.

The interannual variations of the percentage of total observations by year represented by each 700-hPa type are depicted in Fig. 8. Types b, g, and a have increasing frequencies, while Types f, h, d, e, and c have decreasing frequencies. However, only the trends for Types b, g, f, and h ($p < 0.0001$, $r = 0.587$, $p = 0.0187$, $r = 0.370$, $p = 0.0013$, $r = 0.492$, and $p = 0.0002$, $r = 0.563$, respectively) are statistically significant. The strongly and significantly increasing frequency of 700-hPa Type b (CH) is likely to contribute to the marginally-increasing frequency of 1000-hPa Types e (CR/GR) and g (GH) by steering the CR/GR airflow around its periphery and capturing the surface GH beneath its subsiding motion. Types a and c have the smallest frequencies and appear most typically in summer, with very little change over the 40 years. Both types have a trough over the GoM, which supports severe weather formation on the downwind (i.e., eastern) side of the trough axis as the upper-level divergence on the trough-to-ridge side of the Rossby wave encourages lifting beneath it, facilitating storm growth. Therefore, the absence of observed temporal trends in frequency of 1000-hPa FOR- and FGR-like types is accompanied by an absence of significant trends in 700-hPa support for such surface fronts.

4. Link to prescribed burn conditions

The anticyclonic circulation associated with 1000-hPa Types a and c (Fig. 4a and c, respectively) and counter-clockwise circulation associated with low pressure to the east of coastal Texas/Louisiana (Type b; Fig. 3b) would all support offshore flow over the western part of the U.S. GoM coast. Such flow would prevent air quality deterioration over near-coastal populated areas during burns. Neither of these types have displayed significant frequency trends from 1979 to 2018. Higher in the atmosphere, optimal conditions for burns in these locations are associated with 700-hPa Types a and g, which both send air southeastward on the ridge-to-trough side of the Rossby wave over coastal Texas and Louisiana, with Type g becoming more frequent over the 1979–2018 period. Least desirable burn conditions over the western Gulf are likely associated with 1000-hPa Types e, f, and h, which all have anticyclones east of the region and southerly flow that would advect burn residue inland. Of these, Type e is becoming more frequent temporally over the 1979–2018 period. At the 700-hPa level, the clockwise circulation around the high heights/pressure associated with Types b, c, e, and h (Fig. 7b, c, 7e, and 7h) would be likely to advect such burn residue onshore in these places. Of these, Type b may be elicit the most concern, if its very strongly increasing temporal trend in frequency continues into the future. On the other hand, the decreasing frequency of 700-hPa Type h could buffer such effects if it continues.

For the eastern half of the U.S. GoM arc, 1000-hPa geopotential height gradients are generally weaker for most types, suggesting gentle airflow, and/or paralleling the Florida GoM shore. Thus, the situation is more ambiguous. Types e (Fig. 3e) and h (Fig. 3h) present the strongest evidence for (favorable) offshore flow from peninsular Florida's GoM coast, but (unfavorable) onshore flow in the Florida panhandle, Alabama, and Mississippi. At the 700-hPa level, most of the patterns put peninsular Florida either under an anticyclone, thereby causing subsidence and low mixing heights, or on west-to-east flow, which would advect burn residue inland. Type a (Fig. 6a), with its weak height gradient and trough-to-ridge flow, may offer the best opportunity for uplift and gentle venting. In the Florida panhandle, Alabama, and Mississippi, the most favorable burn conditions are associated with the

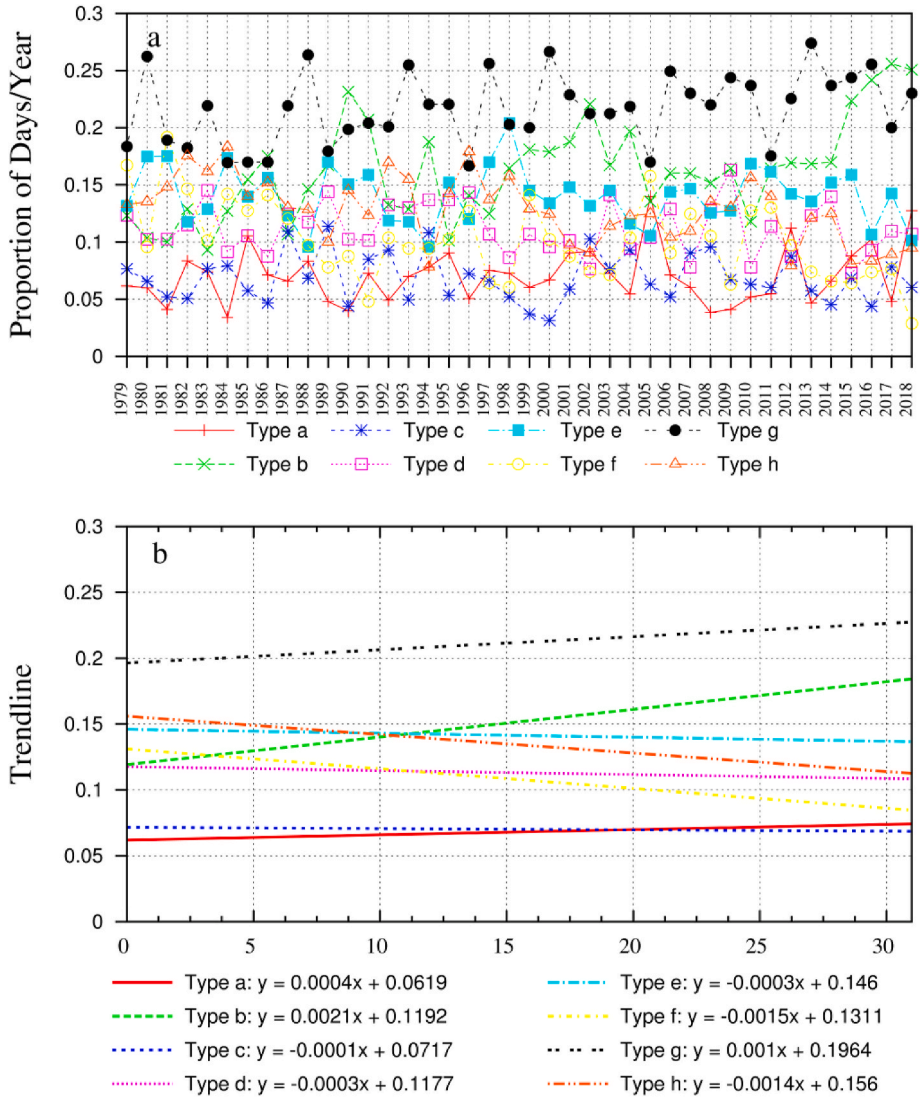

Fig. 8. As in Fig. 5, but for the 700-hPa level.

offshore flow of Type g (Fig. 6g). Because of the gentle synoptic pressure gradients, it is likely that the daily meso-scale land-sea breeze phenomenon may provide better indication of the favorability in peninsular Florida than these synoptic patterns. In such circumstances, the offshore flow of the nocturnal and early morning land breeze may provide the most favorable burn conditions, while the onshore flow associated with the afternoon sea breeze would be far less favorable.

5. Summary/conclusions

Synoptic climatological classification can assist in identifying frequencies and trends in those frequencies of weather types, which can assist wildlife managers in planning for more successful prescribed marsh burns on the U.S. GoM coast. In this research, eight near-surface (i.e., 1000-hPa-level) circulation types and eight 700-hPa circulation types were identified using eigenvector-based map-pattern classifications, based on 40 years of climatic data centered on the GoM coast of the United States. The resulting surface synoptic patterns corroborate those identified in previous research that utilized manual, subjective methods or correlation-based methods and offer a new classification for the 700-hPa level. Surface patterns that situate an anticyclone west of the western GoM arc or a cyclone east of the western GoM arc are most favorable, while the gentle flow in peninsular Florida or presence beneath the BASA may make the mesoscale land-sea breeze phenomenon a better guide to burn favorability than synoptic patterns. Future research should pair up historical burn assessment data with the synoptic types derived here, for validating the suggestions from this research.

Funding

This paper is a result of research funded by the National Oceanic and Atmospheric Administration's RESTORE Science Program under award NA19NOS4510195 to Mississippi State University.

References

Barnston, A. G., & Livezey, R. E. (1987). Classification, seasonality, and persistence of low frequency atmospheric circulation patterns. *Monthly Weather Review, 115*(6), 1083–1126. https://doi.org/10.1175/1520-0493(1987)115<1083:CSAPOL>2.0.CO;2

Beck, C. (2015). Automated synoptic classifications. In S. Elias (Ed.), *Reference module in earth systems and environmental sciences*. Elsevier. https://doi.org/10.1016/B978-0-12-409548-9.09520-8.

Black, A. E., Hayes, P., & Strickland, R. (2020). Organizational learning from prescribed fire escapes: A review of developments over the last 10 years in the USA and Australia, 59 *Current Forestry Reports, 6*(1), 41. https://doi.org/10.1007/s40725-019-00108-0.

Buell, C. E. (1979). On the physical interpretation of empirical orthogonal functions. In *Sixth conference on probability and statistics in atmospheric science* (pp. 112–117). Boston, MA: American Meteorological Society.

Cattell, R. B. (1966). Scree test for number of factors. *Multivariate Behavioral Research, 1*(2), 245–276. https://doi.org/10.1207/s15327906mbr0102_10

Chiodi, A. M., Larkin, N. K., & Varner, J. M. (2018). An analysis of southeastern US prescribed burn weather windows: Seasonal variability and El Niño associations. *International Journal of Wildland Fire, 27*(3), 176–189. https://doi.org/10.1071/WF17132

Chiodi, A. M., Larkin, N. K., Varner, J. M., & Hiers, J. K. (2019). Sensitivity of prescribed burn weather windows to atmospheric dispersion parameters over southeastern USA. *International Journal of Wildland Fire, 28*(8), 589–600. https://doi.org/10.1071/WF18209

Copernicus Climate Change Service (C3S). (2017). *ERA5: Fifth generation of ECMWF atmospheric reanalyses of the global climate. Copernicus climate change Service climate data store (CDS)*. Last accessed https://cds.climate.copernicus.eu/cdsapp#!/home. (Accessed 15 June 2021).

Crisp, C. A., & Lewis, J. M. (1992). Return flow in the Gulf of Mexico. Part I: A classificatory approach with a global historical perspective. *Journal of Applied Meteorology, 31*(8), 868–881. https://doi.org/10.1175/1520-0450(1992)031<0868:RFITGO>2.0.CO;2

Dagg, M. G. (1988). Physical and biological responses to the passage of a winter storm in the coastal and inner shelf waters of the northern Gulf of Mexico. *Continental Shelf Research, 8*(2), 167–178. https://doi.org/10.1016/0278-4343(88)90052-0

Daigle, A., St-Hilaire, A., Beveridge, D., Caissie, D., & Benyahya, L. (2011). Multivariate analysis of the low-flow regimes in eastern Canadian rivers. *Hydrological Sciences Journal, 56*(1), 51–67. https://doi.org/10.1080/02626667.2010.535002

Davis, R. E., & Kalkstein, L. S. (1990). Development of an automated spatial synoptic climatological classification. *International Journal of Climatology, 10*(8), 769–794. https://doi.org/10.1002/joc.3370100802

Dixon, P. G., Goodrich, G. B., & Cooke, W. H. (2008). Using teleconnections to predict wildfires in Mississippi. *Monthly Weather Review, 136*(7), 2804–2811. https://doi.org/10.1175/2007MWR2297.1

Duerr, A. E., Miller, T. A., Lanzone, M., Brandes, D., Cooper, J., O'Malley, K., et al. (2015). Flight response of slope-soaring birds to seasonal variation in thermal generation. *Functional Ecology, 29*(6), 779–790. https://doi.org/10.1111/1365-2435.12381

Engle, M. A., Tate, M. T., Krabbenhoft, D. P., Kolker, A., Olson, M. L., Edgerton, E. S., et al. (2008). Characterization and cycling of atmospheric mercury along the central US Gulf Coast. *Applied Geochemistry, 23*(3), 419–437. https://doi.org/10.1016/j.apgeochem.2007.12.024

Feher, L. C., Allain, L. K., Osland, M. J., Pigott, E., Reid, C., & Latiolais, N. (2021). A comparison of plant communities in restored, old field, and remnant coastal prairies. *Restoration Ecology, 29*(3), Article e13325. https://doi.org/10.1111/rec.13325

Field, D. W., Alexander, C. E., & Broutman, M. (1988). Toward developing an inventory of U.S. coastal wetlands. *Marine Fisheries Review, 50*(1), 40–46.

Frakes, B., & Yarnal, B. (1997). A procedure for blending manual and correlation-based synoptic classifications. *International Journal of Climatology, 17*(13), 1381–1396. https://doi.org/10.1002/(SICI)1097-0088(19971115)17:13<1381::AID-JOC204>3.0.CO;2-Q

Goodrick, S. L., & Hanley, D. (2009). Revisiting the relationship between Florida wildfire activity and ENSO. *International Journal of Wildland Fire, 18*, 476–482. https://doi.org/10.1071/WF07034

Gore, P. A., Jr. (2000). Average linkage method. In H. E. Tinsley, & S. D. Brown (Eds.), *Handbook of applied multivariate statistics and mathematical modeling* (pp. 297–321). San Diego: Academic Press. https://doi.org/10.1016/B978-012691360-6/50012-4.

Hiscox, A., & Flecher, S. (2016). Introducing a smoke prediction tool for small scale agricultural burn management. *Southeastern Geographer, 56*(3), 297–319. https://doi.org/10.1353/sgo.2016.0035

Jackson, J. E. (2005). *A user's guide to principal components* (Vol. 587). Hoboken, NJ: John Wiley & Sons.

Jolliffe, I. T. (1995). Rotation of principal components: Choice of normalization constraints, 35 *Journal of Applied Statistics, 22*(1), 29. https://doi.org/10.1080/757584395.

Jolliffe, I. T. (2002). *Principal component analysis* (2nd ed.). New York: Springer.

Jolliffe, I. T., & Cadima, J. (2003). Principal component analysis: A review and recent developments, 20150202 *Philosophical Transactions of the Royal Society A: Mathematical, Physical & Engineering Sciences, 374*(2065). https://doi.org/10.1098/rsta.2015.0202.

Kalkstein, L. S., Nichols, M. C., Barthel, C. D., & Greene, J. S. (1996). A new spatial synoptic classification: Application to air-mass analysis, 1004 *International Journal of Climatology, 16*(9), 983. https://doi.org/10.1002/(SICI)1097-0088(199609)16:9<983::AID-JOC61>3.0.CO;2-N.

Keim, B. D., & Muller, R. A. (1992). Temporal fluctuations of heavy rainfall magnitudes in New Orleans, Louisiana 1871–1991, 730 *Water Resources Bulletin, 28*(4), 721. https://doi.org/10.1111/j.1752-1688.1992.tb01494.x.

Köppen, W. (1884). Die Wärmezonen der Erde, nach der Dauer der heissen, gemässigten und kalten Zeit und nach der Wirkung der Wärme auf die organische Welt betrachtet. (The warm zones of the earth, considered according to the duration of the hot, moderate and cold times and according to the effect of heat on the organic world). *Meteorologische Zeitschrift, 1*(21), 5–226.

Kostopoulou, E., & Jones, P. D. (2007). Comprehensive analysis of the climate variability in the eastern mediterranean. Part I: Map-pattern classification. *International Journal of Climatology, 27*(9), 1189–1214. https://doi.org/10.1002/joc.1467

Labosier, C. F., Frauenfeld, O. W., Quiring, S. M., & Lafon, C. W. (2015). Weather type classification of wildfire ignitions in the central Gulf Coast, United States. *International Journal of Climatology, 35*(9), 2620–2634. https://doi.org/10.1002/joc.4160

Lewis, J. M., & Crisp, C. A. (1992). Return flow in the Gulf of Mexico. Part II: Variability in return flow thermodynamics inferred from trajectories over the Gulf. *Journal of Applied Meteorology, 31*(8), 882–898. https://doi.org/10.1175/1520-0450(1992)031<0882:RFITGO>2.0.CO;2

Lewis, A. B., & Keim, B. D. (2015). A hybrid procedure for classifying synoptic weather types for Louisiana, USA. *International Journal of Climatology, 35*(14), 4247–4261. https://doi.org/10.1002/joc.4283

Liu, Y., & Weisberg, R. H. (2005). Patterns of ocean current variability on the West Florida Shelf using the self-organizing map. *Journal of Geophysical Research, 110*. https://doi.org/10.1029/2004JC002786. C06003.

Liu, Y., & Weisberg, R. H. (2011). A review of self-organizing map applications in meteorology and oceanography. In J. I. Mwasiagi (Ed.), *Self-organizing maps - applications and novel algorithm design* (pp. 253–272). Rijeka, Croatia: InTech, ISBN 978-953-307-546-4.

McCarty, J. L., Korontzi, S., Justice, C. O., & Laboda, T. (2009). The spatial and temporal distribution of crop residue burning in the contiguous United States. *The Science of the Total Environment, 407*(21), 5701–5712. https://doi.org/10.1016/j.scitotenv.2009.07.009

Melvin, M. A. (2020). 2020 national prescribed fire use report. In *Technical bulletin 04-20. Coalition of prescribed fire councils*, 15 June 2021 https://www.stateforesters.org/wp-content/uploads/2020/12/2020-Prescribed-Fire-Use-Report.pdf.

Mo, K. C., & Berbery, E. H. (2004). Low-level jets and the summer precipitation regimes over North America. *Journal of Geophysical Research: Atmosphere, 109*. https://doi.org/10.1029/2003JD004106. D06117.

Muller, R. A. (1977). A synoptic climatology for environmental baseline analysis: New Orleans. *Journal of Applied Meteorology, 16*(1), 20–33. https://doi.org/10.1175/1520-0450(1977)016<0020:ASCFEB>2.0.CO;2

Muller, R. A., & Jackson, A. L. (1985). Estimates of climatic air-quality potential at Shreveport, Louisiana. *Journal of Climate and Applied Meteorology, 24*(4), 293–301. https://doi.org/10.1175/1520-0450(1985)024<0293:EOCAQP>2.0.CO;2

Nyman, J. A., & Chabreck, R. H. (1995). Fire in coastal marshes: History and recent concerns. Available at:. In S. I. Cerulean, & R. T. Engstrom (Eds.), *Proceedings 19th tall timbers fire ecology conference- fire in wetlands: A management perspective* (pp. 134–141). Tall Timbers Research, Inc. Tallahassee, Florida. Last accessed: 15 June 2021 http://talltimbers.org/wp-content/uploads/2014/03/NymanandChabreck1995_op.pdf.

Overland, J. E., & Preisendorfer, R. W. (1982). A significance test for principal components applied to a cyclone climatology. *Monthly Weather Review, 110*(1), 1–4. https://doi.org/10.1175/1520-0493(1982)110<0001:ASTFPC>2.0.CO;2

Pandžić, K. (1988). Principal component analysis of precipitation in the Adriatic-Pannonian area of Yugoslavia. *Journal of Climatology, 8*(4), 357–370. https://doi.org/10.1002/joc.3370080404

Raziei, T., Bordi, I., Santos, J. A., & Mofidi, A. (2013). Atmospheric circulation types and winter daily precipitation in Iran. *International Journal of Climatology, 33*(9), 2232–2246. https://doi.org/10.1002/joc.3596

Richman, M. B. (1986). Rotation of principal components. *Journal of Climatology, 6*(3), 293–335. https://doi.org/10.1002/joc.3370060305

Richman, M. B., & Lamb, P. J. (1985). Climatic pattern analysis of three- and seven-day summer rainfall in the central United States: Some methodological considerations and a regionalization. *Journal of Climate and Applied Meteorology, 24*(12), 1325–1343. https://doi.org/10.1175/1520-0450(1985)024<1325:CPAOTA>2.0.CO;2

Rohli, R. V., & Henderson, K. G. (1998). Upper-level steering flow and continental anticyclones on the central Gulf Coast of the United States. *International Journal of Climatology, 18*(9), 935–954. https://doi.org/10.1002/(SICI)1097-0088(199807)18:9<935::AID-JOC299>3.0.CO;2-U

Rohli, R. V., & Henderson, K. G. (2002). A comparison of 500 hPa height patterns associated with anticyclones of Pacific and continental origin impacting the Central Gulf Coast, United States. *Physical Geography, 23*(6), 449–464. https://doi.org/10.2747/0272-3646.23.6.449

Rohli, R. V., & Rogers, J. C. (1993). Atmospheric teleconnections and citrus freezes in the southern United States. *Physical Geography, 14*(1), 1–15. https://doi.org/10.1080/02723646.1993.10642464

Rohli, R. V., Russo, M. M., Vega, A. J., & Cole, J. B. (2004). Tropospheric ozone in Louisiana and synoptic circulation. *Journal of Applied Meteorology, 43*(10), 1438–1451. https://doi.org/10.1175/JAM2137.1

Sheridan, S. C. (2002). The redevelopment of a weather-type classification scheme for North America. *International Journal of Climatology, 22*(1), 51–68. https://doi.org/10.1002/joc.709

Trenberth, K. E., Stepaniak, D. P., & Caron, J. M. (2000). The global monsoon as seen through the divergent atmospheric circulation. *Journal of Climate, 13*(22), 3969–3993. https://doi.org/10.1175/1520-0442(2000)013<3969:TGMAST>2.0.CO;2

Unglert, K., Radić, V., & Jellinek, A. M. (2016). Principal component analysis vs. self-organizing maps combined with hierarchical clustering for pattern recognition in volcano seismic spectra, 2016 *Journal of Volcanology and Geothermal Research, 320*, 58–74. https://doi.org/10.1016/j.jvolgeores.2016.04.014.

Van Lear, D. H., Carroll, W. D., Kapeluck, P. R., & Johnson, R. (2005). History and restoration of the longleaf pine-grassland ecosystem: Implications for species at risk. *Forest Ecology and Management, 211*(1–2), 150–165. https://doi.org/10.1016/j.foreco.2005.02.014

Vega, A. J., Rohli, R. V., & Henderson, K. G. (1998). The Gulf of Mexico mid-tropospheric response to El Niño and La niña forcing. *Climate Research, 10*(2), 115–125. https://doi.org/10.3354/cr010115

Wang, F. C., Ransibrahmanakul, V., Tuen, K. L., Wang, M. L., & Zhang, F. (1995). Hydrodynamics of a tidal inlet in fourleague Bay atchafalaya Bay, Louisiana. *Journal of Coastal Research, 11*(3), 733–743.

Wang, X. L., Xu, J. Y., Wu, Z. S., Shen, Y. C., & Cai, Y. J. (2019). Effect of prescribed burning of wetlands on soil organic carbon fractions: A 5-year study in poyang, China, 2019 *Ecological Engineering, 138*, 219–226. https://doi.org/10.1016/j.ecoleng.2019.07.028.

Ward, J. H. (1963). Hierarchical grouping to optimize an objective function. *Journal of the American Statistical Association, 58*(301), 236–244. https://doi.org/10.2307/2282967

Whitehead, S., Weald, H., & Baines, D. (2021). Post-burning responses by vegetation on blanket bog peatland sites on a Scottish grouse moor, 107336 *Ecological Indicators, 123*. https://doi.org/10.1016/j.ecolind.2021.107336.

Yarnal, B. (1993). *Synoptic climatology in environmental analysis*. London: Belhaven Press.

Yarnal, B., Comrie, A. C., Frakes, B., & Brown, D. P. (2001). Developments and prospects in synoptic climatology. *International Journal of Climatology, 21*(15), 1923–1950. https://doi.org/10.1002/joc.675

Yim, O., & Ramdeen, K. T. (2015). Hierarchical cluster analysis: Comparison of three linkage measures and application to psychological data. *The Quantitative Methods for Psychology, 11*(1), 8–21. https://doi.org/10.20982/tqmp.11.1.p008

Zscheischler, J., Mahecha, M. D., & Harmeling, S. (2012). Climate classifications: The value of unsupervised clustering. *Procedia Computer Science, 9*, 897–906. https://doi.org/10.1016/j.procs.2012.04.096